

Nanoscale

Accepted Manuscript



This is an *Accepted Manuscript*, which has been through the Royal Society of Chemistry peer review process and has been accepted for publication.

Accepted Manuscripts are published online shortly after acceptance, before technical editing, formatting and proof reading. Using this free service, authors can make their results available to the community, in citable form, before we publish the edited article. We will replace this *Accepted Manuscript* with the edited and formatted *Advance Article* as soon as it is available.

You can find more information about *Accepted Manuscripts* in the [Information for Authors](#).

Please note that technical editing may introduce minor changes to the text and/or graphics, which may alter content. The journal's standard [Terms & Conditions](#) and the [Ethical guidelines](#) still apply. In no event shall the Royal Society of Chemistry be held responsible for any errors or omissions in this *Accepted Manuscript* or any consequences arising from the use of any information it contains.



Synthesis of hierarchical porous δ -MnO₂ nanoboxes as an efficient catalyst for rechargeable Li–O₂ battery

Received 00th January 20xx,
Accepted 00th January 20xx

DOI: 10.1039/x0xx00000x

www.rsc.org/

Jian Zhang,^{a,b} Yanping Luan,^b Zhiyang Lyu,^b Liangjun Wang,^c Leilei Xu,^b Kaidi Yuan,^c Feng Pan,^b Min Lai,^a Zhaolin Liu,^{*d} and Wei Chen^{*b,c,e}

Rechargeable lithium-oxygen (Li–O₂) battery with remarkably high theoretical energy storage capacity has attracted enormous research attention. However, the poor oxygen reduction and oxygen evolution reactions (ORR and OER) activities in discharge and charge processes cause low energy efficiency, poor electrolyte stability and short cycle life. This requires the development of efficient cathode catalysts to dramatically improve the Li–O₂ battery performances. MnO₂-based materials are recognized as efficient and low-cost catalysts for Li–O₂ battery cathode. Here, we report a controllable approach to synthesize hierarchical porous δ -MnO₂ nanoboxes by using Prussian blue analogues as the precursors. The obtained products possess hierarchical pore size and extremely large surface area (249.3 m² g⁻¹), which would favour the oxygen transportation and provide more catalytic active sites to promote ORR and OER as Li–O₂ battery cathode. The battery shows enhanced discharge capacity (4368 mAh g⁻¹@0.08 mA cm⁻²), reduced overpotential (270 mV), improved rate performance and excellent cycle stability (248 cycles@500 mAh g⁻¹ and 112 cycles@1000 mAh g⁻¹), in comparison with the battery with VX-72 carbon cathode. The superb performance of the hierarchical porous δ -MnO₂ nanoboxes, together with the convenient fabrication method, presents an alternative to develop advanced cathode catalysts for Li–O₂ battery.

1. INTRODUCTION

With the rapid development of intermittent renewable energies and sustainable electric transportation energy sources, energy storage systems with ultra-high-energy-density and long-lasting service life are highly desirable. Extensive research efforts have been devoted to developing next-generation energy storage systems, e.g., rechargeable Li–O₂ battery, for their remarkably high theoretical energy density.^{1–4} The theoretical energy density of Li–O₂ battery is about 3500 Wh/kg, which is 4 to 6 times higher than that of traditional Li-ion batteries.^{5–7} However, for the practical applications, Li–O₂ battery has suffered numerous challenges during the discharge-charge process,^{8,9} e.g., the high overpotential that dramatically lowers the discharge-charge cycle efficiency; the poor electrolyte and cathode stability that reduce

the cycle life; and the insulating nature of discharge product (Li₂O₂) that limits the discharge capacity at high currents.¹⁰ It has been suggested that the key to solve these problems is to develop highly-efficient cathode electrocatalysts, as cathode reaction in Li–O₂ battery is generally a catalytically electrochemical process.¹¹ A variety of materials have been developed and employed as the cathode catalysts, ranging from noble metals and noble metal oxides to carbon-based materials, transition-metal oxides and soluble additives.^{12–16} Transition metal oxides with relatively low cost, high chemical stability and considerable high catalytic activity have shown comparative advantages as cathode catalysts for Li–O₂ battery.^{17–20} Among all the transition metal oxides, MnO₂-based catalysts with high catalytic ability, and controllable size, morphology and structure have attracted much attention.

Bruce and co-workers systematically studied the catalytic performance of various manganese oxides and predicted that α -MnO₂ showed best performance for the application of Li–O₂ battery.²¹ Since then, various strategies have been developed to synthesize MnO₂-based materials for high performance Li–O₂ battery, such as controlling morphology and crystalline states,^{22–25} growth on different substrates (conductive carbon,^{26, 27} graphene,^{28–31} Ni foam^{32, 33} etc), as well as decoration by noble metals^{34–36} and other metal oxide³⁷. Among them, δ -MnO₂ with two-dimension (2D) lamellar structure has been widely investigated as the substrate material, decorated material and catalyst in the application of Li–O₂ battery and all of them shows reduced overpotential, improved cycle performance and good rate performance.^{38–40} In addition, porous materials, especially porous

^aSchool of Physics and Optoelectronic Engineering, Nanjing University of Information Science & Technology, Nanjing 210044, Jiangsu, China

^bDepartment of Chemistry, National University of Singapore 3 Science Drive 3, 117543, Singapore. E-mail: phvcw@nus.edu.sg

^cDepartment of Physics National University of Singapore 2 Science Drive 3, 117542 Singapore

^dInstitute of Materials Research & Engineering, 3 Research Link, Singapore 117602, Singapore. E-mail: zl-liu@imre.a-star.edu.sg

^eNational University of Singapore (Suzhou) Research Institute, 377 Lin Quan Street, Suzhou Industrial Park, Jiangsu Prov. 215123, China

Electronic Supplementary Information (ESI) available: [details of any supplementary information available should be included here]. See DOI: 10.1039/x0xx00000x

hollow structured materials are favourable in Li-O₂ battery, as they can facilitate the transportation of oxygen and electrolyte, as well as minimize the undesirable clogging of the air cathode.⁴¹⁻⁴⁶ Furthermore, porous hollow materials with large surface area can provide sufficient catalytic active sites to promote the oxygen reduction reaction/oxygen evolution reaction (ORR/OER). However, up to now, there has been limited success in the synthesis of hollow structured MnO₂ with large surface area.

Recently, Prussian blue analogues (PBAs) with controlled structure have been recognized as promising precursors to synthesize porous metal oxide.⁴⁷⁻⁵⁰ Lou and his colleagues have successfully developed a series of Fe-based metal oxide by using Fe₄[Fe(CN)₆]₃ as the sacrificial precursors.⁵¹⁻⁵³ Chen et al. also have paved the way for the synthesis of various metal oxides (such as Co₃O₄, Fe_xCo_{3-x}O₄, CuO/Cu₂O etc) based on the PBAs templates.^{49, 54-56} Particularly, the metal oxides derived from PBAs usually exhibit desired morphology, large surface area, uniform pore structure and

hierarchical pore size.^{47, 49} All of these features are crucial to design efficient cathode catalysts for Li-O₂ battery.

In the present study, hierarchical porous δ -MnO₂ nanoboxes were synthesized by a controllable routine deriving from PBAs, which presented co-existing meso-macropores and extremely large surface area up to 249.3 m² g⁻¹. When employed as the cathode catalyst of Li-O₂ battery, the hierarchical porous δ -MnO₂ nanoboxes electrode can deliver a high discharge capacity of 4368 mAh g⁻¹ with reduced overpotentials up to 270 mV compared with commercial Vulcan XC-72 carbon electrode at 0.08 mA cm⁻², and enhanced specific capacity and capacity retention were also obtained at various current densities. At a rate of 0.16 mA cm⁻², the battery with hierarchical porous δ -MnO₂ nanoboxes catalyst possessed long cycle stability up to 248 cycles and 112 cycles without obvious capacity decay at the limited discharge capacity of 500 mAh g⁻¹ and 1000 mAh g⁻¹, respectively.

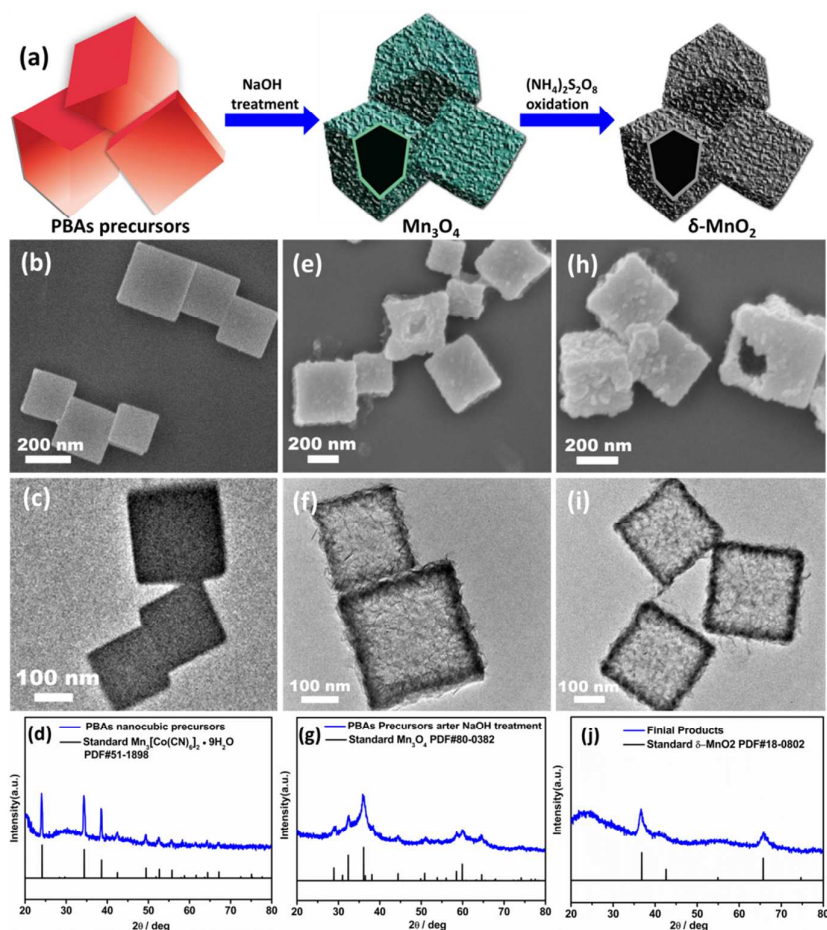


Fig. 1 (a) Schematic illustration of the formation of the hierarchical porous δ -MnO₂ nanoboxes; SEM images (b, e, h), TEM images (c, f, i) and XRD patterns (d, g, j) of the obtained nanocube-like PBAs precursors (b, c, d), porous Mn₃O₄ nanoboxes (e, f, g) and hierarchical porous δ -MnO₂ nanoboxes (h, i, j).

2. Experiments

2.1 Synthesis Procedures

Synthesis of PBAs precursors: The nanocube-like PBAs precursors were synthesized via modified self-assembly method.^{57, 58} Firstly, 0.6 g polyvinyl pyrrolidone (PVP) and 0.0372 g $\text{Mn}(\text{CH}_3\text{COO})_2 \cdot 4\text{H}_2\text{O}$ were dissolved in 7 ml deionized (DI) water and 30 ml absolute ethanol to form a transparent solution. Then, 20 ml of 0.04 mmol $\text{K}_3[\text{Co}(\text{CN})_6]$ was added dropwise into the above solution by using a syringe at the rate of 0.1 ml min^{-1} . The mixed solution was kept under room temperature for 24 h. The resulting white precipitate was collected and washed several times with absolute ethanol, and then dispersed into 20 ml of ethanol for further use.

Synthesis of Mn_3O_4 nanoboxes: Mn_3O_4 nanoboxes were obtained by the reaction of $\text{Mn}_3[\text{Co}(\text{CN})_6]_2 \cdot 9\text{H}_2\text{O}$ with NaOH at room temperature. Typically, 200 ml of 0.001M NaOH solution was added to above $\text{Mn}_3[\text{Co}(\text{CN})_6]_2 \cdot 9\text{H}_2\text{O}$ nanocubes suspension and stirred for 5 mins. After that, the as-prepared product was collected and washed with absolute ethanol and DI water, and finally dried in an oven at 80°C. For synthesis of the different morphology of Mn_3O_4 , NaOH solution with different concentration (0.0005M, 0.002M, 0.005M, 0.01M, 0.02 M, 0.05 M) was used.

Synthesis of hierarchical porous $\delta\text{-MnO}_2$ nanoboxes: MnO_2 nanoboxes were obtained by the reaction of Mn_3O_4 with $(\text{NH}_4)_2\text{S}_2\text{O}_8$. Firstly, 50 ml of 0.5 M $(\text{NH}_4)_2\text{S}_2\text{O}_8$ aqueous solution was prepared and the pH of the solution was then adjusted to about 8-9. 50 mg Mn_3O_4 was added to the above solution. After that, the mixture was stirred at 80 °C for 8 h. The final product was collected and washed with absolute ethanol and DI water several times. Finally the products were dried in an oven at 80°C.

2.2 Instruments for Characterization

The morphology of the as-prepared samples was examined by scanning electron microscope (SEM) on JEOL JSM 6700F and transmission electron microscope (TEM) on a JEOL 2010 microscope. The composition of the samples was analyzed by energy-dispersive X-ray spectroscopy (EDX) attached to the TEM instrument. The X-ray diffraction (XRD) patterns of the samples were collected from a PANalytical Empyrean DY 708 diffractometer with Cu radiation ($\text{Cu K}\alpha=0.15406$ nm). Fourier transform-infrared spectroscopy (FT-IR) was carried out on FT-IR Spectrum 2000 (PerkinElmer) and Varian 3100 FT-IR. Brunauer-Emmett-Teller (BET) surface area was measured by nitrogen sorption at 77 K on a surface area & pore size analyzer (NOVA 2200e). X-ray photoelectron spectroscopy (XPS) analyses were performed on XR 50 HP X-ray source and Phoibos HSA3500 analyzer.

2.3 Li-O₂ cell assembly and battery test

Generally, the catalyst slurry was prepared by mixing 40% catalysts with 50% Vulcan XC-72 (VX-72) carbon (Cabot Carbon Ltd) and 10% polyvinylidene fluoride (PVDF), or 90% VX-72 carbon with 10% PVDF. The air cathodes were fabricated by coating the catalyst slurry on carbon paper current collector homogeneously. The mass loading of the slurry on the cathode was about 0.8-1.2 mg cm^{-2} , and the discharge capacity was calculated based on the total weight of the catalyst and carbon additives. All the Li-O₂ batteries were

assembled by using coin cells in glove box under Argon atmosphere. Glass fiber membranes were used as the separator and 1 M lithium trifluoromethanesulfonate/tetraethylene glycol dimethyl ether ($\text{LiCF}_3\text{SO}_3/\text{TEGDME}$) was used as the electrolyte. Galvanostatic discharge-charge test of the Li-O₂ battery was carried out on LAND multi-channel battery testing system.

3. Results and Discussions

3.1 Synthesis, Morphological, Structural Characterization

Fig. 1 shows the schematic of the synthesis process and corresponding characterizations of the obtained hierarchical porous $\delta\text{-MnO}_2$ nanoboxes. As schematically displayed in Fig. 1a, the fabrication process was carried out through a three-step route. In the first step, nanosized PBAs precursors were synthesized by a self-assembly method,^{57, 58} and possessed smooth facets and well-defined cubic shape with size ranging from 150 to 250 nm, as shown in the scanning electron microscope (SEM) and transmission electron microscope (TEM) images (Fig. 1b, 1c and Fig. S1a). The X-ray diffraction (XRD) pattern (Fig. 1d) demonstrated that these precursors were $\text{Mn}_3[\text{Co}(\text{CN})_6]_2 \cdot 9\text{H}_2\text{O}$ (PDF#51-1989). In the next step, intermediate product with hollow nanoboxes structure (Fig. 1e, 1f and Fig. S1b) was obtained by a precisely controlled reaction between the PBAs precursors and NaOH alkaline solution (0.001M). In the alkaline solution, ion exchange reaction was happened as described below: $\text{Mn}_3[\text{Co}(\text{CN})_6]_2(\text{s}) + 6\text{OH}^-(\text{aq}) \rightarrow 3\text{Mn}(\text{OH})_2(\text{s}) + 2\text{Co}(\text{CN})_6^{3-}$. The ion exchange reaction was verified by the fourier transform-infrared spectroscopy (FT-IR) and x-ray photoelectron spectroscopy (XPS) analysis in Fig. S2. The dominant peaks at 2170 cm^{-1} attributed to CN stretching in the FT-IR spectrum and N 1s peak at 397.8 eV in the XPS disappeared after the ion exchange reaction, which indicated the removal of the $\text{Co}(\text{CN})_6^{3-}$ group from the PBAs precursors. The EDX spectra also show the disappearance of cobalt content after the NaOH treatment (Fig. S3), further evidencing the ion exchange reaction between $\text{Co}(\text{CN})_6^{3-}$ and OH^- . The as-prepared intermediate nanoboxes was indexed to Mn_3O_4 (PDF#80-0382) instead of $\text{Mn}(\text{OH})_2$ by the XRD measurement (Fig. 1g). This was due to the fact that $\text{Mn}(\text{OH})_2$ can be easily oxidized by oxygen during the self-assembly reaction and drying process.^{59, 60} The XPS measurements further confirm the formation of Mn_3O_4 (Fig. S4a). The two peaks with binding energies of 641.5 and 652.8 eV can be assigned to $\text{Mn}2p_{3/2}$ and $\text{Mn}2p_{1/2}$ of Mn_3O_4 .⁶¹

In the last step, the final products were obtained by oxidizing the hollow Mn_3O_4 nanoboxes with a strong oxidation reagent $(\text{NH}_4)_2\text{S}_2\text{O}_8$ at 80°C. There was negligible change in the shape and size after oxidation (Fig. 1h, 1i and Fig. S1c), indicating the good structural stability of the porous Mn_3O_4 nanoboxes. The XRD pattern of the final product indicated that the porous Mn_3O_4 nanoboxes can be easily converted to $\delta\text{-MnO}_2$ (PDF#18-0802) during the low temperature oxidation process (Fig. 1j). Clear lattice spacing of 0.244 nm was observed in the high-resolution TEM (HR-TEM) image (Fig. 2d), which was in good agreement with the inter-plane spacing of (006) plane of $\delta\text{-MnO}_2$. The selected area electron diffraction (SAED) pattern (Fig. 2c) showed that the $\delta\text{-MnO}_2$ were polycrystalline.

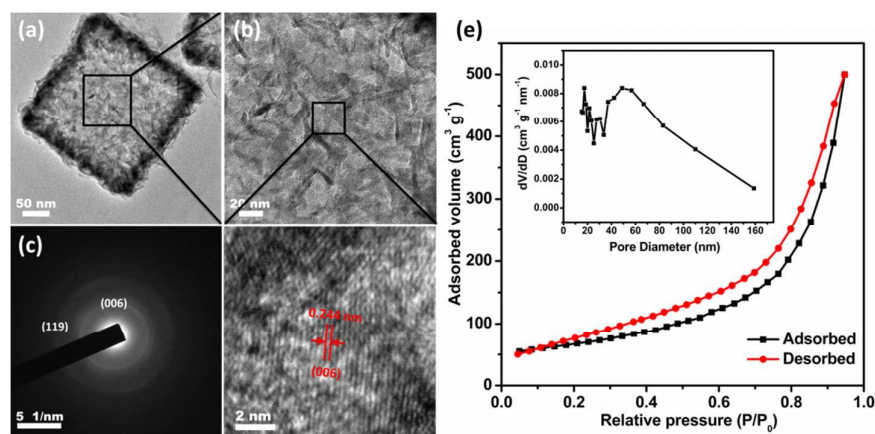


Fig. 2 HR-TEM images (a, b, d) and SAED pattern (c) of hierarchical porous δ -MnO₂ nanoboxes; (e) Nitrogen adsorption–desorption isotherms and pore size distribution (inset) of the hierarchical porous δ -MnO₂ nanoboxes.

The formation of MnO₂ was further confirmed by the XPS measurements (Fig. S4b). The two peaks with binding energies of 642.2 and 653.8 eV corresponded to Mn2p_{3/2} and Mn2p_{1/2} of MnO₂ (Fig. S2b), in good accordance with previous report.^{61–63} It is worth mentioning that our fabrication process was distinct from the conventional synthesis methods, in which the metal oxides were usually obtained through calcination of PBAs precursors in air or O₂.^{49, 55} In our method, all processes were carried out at low temperature. Therefore, the shape and porous structure of the PBAs precursors were well retained and particles aggregation was significantly reduced. The porosity of the δ -MnO₂ nanoboxes was determined by N₂ adsorption-desorption measurement as displayed in Fig. 2e. It could be observed that the isotherm was type IV with H3-shaped hysteresis loops. The BET specific surface area was up to 249.3 m² g⁻¹. To the best of our knowledge, this is the largest surface area among the reported MnO₂ materials.^{64–66} (Table S1) The pore size distribution in the range of 15–158 nm calculated from the Barrett–Joyner–Halenda (BJH) method was shown as inset in Fig. 2e. The mesopores around 20 nm referred to the accumulated pores of inter-nanoboxes and inter-nanosheets on the surface of the nanoboxes, and macropores centered at about 60 nm were related to the inner space of the hollow nanoboxes. The existing of meso- and macropores accounted for a significant pore volume up to 0.825 cm³ g⁻¹. The large surface area and abundant pore volume should arise from the non-calcination fabrication process, which can avoid the serious particles aggregation in the traditional high temperature oxidation process. Such unique porous hollow structure with large surface area favorable in Li-O₂ battery, as they can provide (1) numerous meso- and macro-channels for the access of oxygen and electrolyte to facilitate the rapid diffusion of lithium ions within the electrode and the electrolyte, (2) sufficient catalytic sites to promote the ORR/OER. Even mixed with carbon additives to prepare the cathode, the well defined hollow nanoboxes can act as the framework to build a good porous conducting matrix, which can facilitate the infiltration of the electrolyte and the diffusion of oxygen.

We also investigated the correlation of the morphology of Mn₃O₄ intermediate products with the concentration of NaOH, as shown in Fig. 3. In the low concentration of NaOH solution (≤ 0.001 M), the ion exchange reaction first took place at the interface between the solid PBAs nanocubic precursors and NaOH solution, forming a thin layer of Mn(OH)₂. With the reaction proceeding, OH⁻ ions continued to flow inward slowly to supply the ion exchange reaction, while the precipitation of Mn(OH)₂ sheets on the pre-formed Mn(OH)₂ layer and the outward diffusion of Co(CN)₆³⁻ ions were anticipated.⁵¹ If the supply of OH⁻ is inadequate (0.0005M), the ion exchange reaction was not complete, and the yolk-shelled structural Mn₃O₄ was obtained (Fig. 3a); otherwise, the whole PBAs precursors was consumed and well-defined nanobox was formed (Fig. 1e and 1f). On the contrary, in the high concentration of NaOH solution (>0.001M), the inward diffusion of OH⁻ and the ion exchange reaction can be significantly accelerated, thereby preventing the formation of the Mn(OH)₂ shell, and leading to the growth of Mn(OH)₂ clusters or sheets. For example, at the NaOH concentration of 0.002M, localized Mn(OH)₂ clusters formed and porous structure instead of hollow nanoboxes were obtained (Fig. 3b). At the NaOH concentration of 0.02M, the cubic structure of the precursors was partially destroyed and sheet-like subunits grew significantly (Fig. 3e). When the concentration increased to 0.05M, the cubic morphology disappeared completely and flower-like morphology assembled by ultrathin nanosheets appeared (Fig. 3f). These results revealed that the key to obtain the hollow nanoboxes structure was the precise manipulation of the ion exchange reaction by using the alkaline solution with proper concentration.

3.2 Li-O₂ battery Performance

The battery performance of the hierarchical porous δ -MnO₂ nanoboxes catalyst was evaluated by the galvanostatic charge-discharge measurements in coin cell type Li-O₂ battery cells using lithium chip as the anode and 1 M lithium

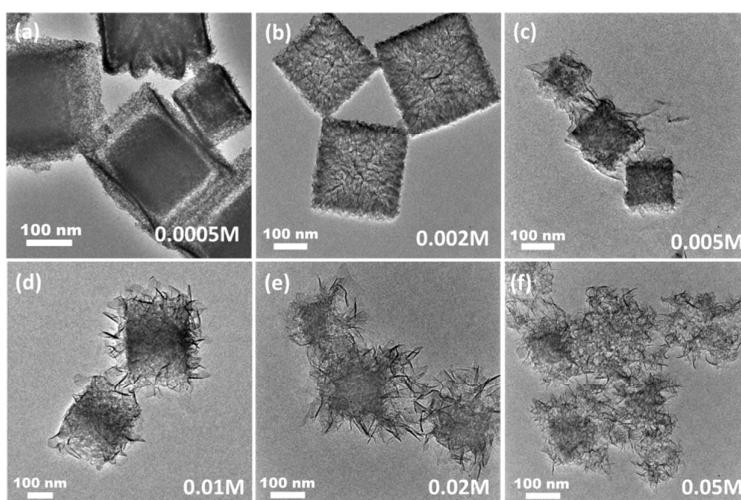


Fig. 3 TEM images of the PBAs precursors after the treatment with NaOH solution with various concentrations: (a) 0.0005M, (b) 0.002M, (c) 0.005M, (d) 0.01M, (e) 0.02M, (f) 0.05M

trifluoromethanesulfonate/tetraethylene glycol dimethylether (LiCF₃SO₃/TEGDME) as the electrolyte.^{20, 67} Commercial Vulcan XC-72 (VX-72) carbon was employed as reference cathode for comparison. VX-72 carbon black was also used as an electrically conductive additive, mixed with hierarchical porous δ -MnO₂ nanoboxes catalyst to form conducting matrix as the air cathode. Fig. 4a shows the first discharge–charge profiles of the Li–O₂ cells with hierarchical porous δ -MnO₂ nanoboxes and VX-72 carbon electrodes at a current density of 0.08 mA cm⁻². It can be seen that the Li–O₂ cell with hierarchical porous δ -MnO₂ nanoboxes electrode exhibited increased discharge plateau voltage and reduced charge plateau voltage, resulting in a reduced overpotential (about 270 mV) compared with the battery with VX-72 carbon electrode. Consequently, enhanced round-trip efficiency (the ratio of discharge to charge voltage) was obtained. The round-trip efficiency of the Li–O₂ cell with the hierarchical porous δ -MnO₂ nanoboxes electrode was about 66.7%, which was higher than that of the VX-72 carbon electrode (61.5%). Another important improvement is that the hierarchical porous δ -MnO₂ nanoboxes electrode showed enhanced discharge capacity. The first discharge capacity of the battery cell with hierarchical porous δ -MnO₂ nanoboxes electrode was 4368 mAh g⁻¹, which is much higher than that of VX-72 carbon electrode (3136 mAh g⁻¹). It should be noted that the specific discharge capacity of the current collector carbon paper was very low (Fig. S5), indicating that carbon paper was basically inactive and had negligible contribution to the discharge capacity in the Li–O₂ battery system. The enhanced capacity was attributed to the higher catalytic activity of hierarchical porous δ -MnO₂ nanoboxes catalyst to promote the ORR. The large surface area of the hierarchical porous δ -MnO₂ nanoboxes also offered sufficient active sites to catalyze the ORR.

The rate performance of hierarchical porous δ -MnO₂ nanoboxes electrode and VX-72 carbon electrode were measured at various current densities, as shown in Fig. 4b and Fig. S6. The batteries with the hierarchical porous δ -MnO₂ nanoboxes electrodes possessed a higher discharge capacity (Fig. 4b) and

higher capacity retention (Fig. S6c) than that of the pure VX-72 carbon electrodes under all investigated current densities. In addition, the charge capacities of the batteries with porous δ -MnO₂ nanoboxes electrodes were close to the discharge capacity at all the investigated current densities (Fig. S6a). Even at the current density of 0.24 mA cm⁻², the Coulombic efficiencies (the ratio of charge capacity to discharge capacity) of the battery was still higher than 90% (Fig. S6d), which indicate the porous δ -MnO₂ nanoboxes electrodes possess high charge efficiency and good rate performance.

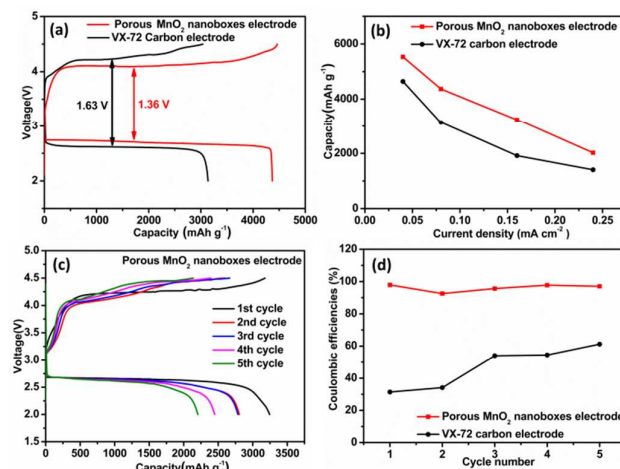


Fig. 4 (a) First discharge–charge curves of Li–O₂ batteries with the hierarchical porous δ -MnO₂ nanoboxes and VX-72 carbon electrodes at 0.08 mA cm⁻²; (b) Discharge capacity of Li–O₂ battery cells with different electrodes at various current densities; (c) Discharge–charge curves of Li–O₂ batteries with hierarchical porous δ -MnO₂ nanoboxes electrode at 0.16 mA cm⁻²; (d) Comparison of the coulombic efficiency of Li–O₂ batteries with different electrodes.

In contrast, the Coulombic efficiencies of the batteries with VX-72 electrodes decreased rapidly with the current density increasing and most of the capacity cannot be recharged at current density of 0.24 mA cm^{-2} (Fig. S6b and S6d). Such improved rate performance could be ascribed to the mesoporous and macroporous structure, which could ensure the easy transportation of oxygen and electrolyte, and thus promote the mass transfer during the formation and decomposition of Li_2O_2 .

The full capacity discharge–charge cycle performance of the Li-O_2 battery was examined at the current density of 0.16 mA cm^{-2} . As shown in Fig. 4c, the Li-O_2 battery with hierarchical porous $\delta\text{-MnO}_2$ nanoboxes electrode possessed the capacity of 3324 mAh g^{-1} at the first discharge process and of 2203 mAh g^{-1} after 5 cycles, showing the capacity retention of 68%. In contrast, the first discharge capacity of the battery with VX-72 electrode was about 1917 mAh g^{-1} and rapid capacity decay was observed during the cycle process with less than 10% capacity retained after 5 discharge–charge cycles (Fig. S7). The XRD pattern evidenced that the main discharge products of the hierarchical porous $\delta\text{-MnO}_2$ nanoboxes electrode after the 5th discharge were Li_2O_2 (Fig. S8a). Li_2CO_3 and $\text{CH}_3\text{CO}_2\text{Li}$ were also observed in the FTIR spectrum (Fig. S8b), which may come from the electrolyte decomposition and side reaction during the discharge-charge process.^{41, 68} Furthermore, the average coulombic efficiency of the battery with hierarchical porous $\delta\text{-MnO}_2$ nanoboxes electrode was as high as 96% during these five cycles, which is much higher than that of battery with VX-72 carbon electrode (50%) (Fig. 4d). This suggested that the hierarchical porous $\delta\text{-MnO}_2$ nanoboxes electrode possessed high charging efficiency during these cycles. The poor charging efficiency of the VX-72 carbon electrode resulted in the incomplete decomposition of the discharge products (Fig. S9a and S9c), and the resistance aggravation of the air cathode (Fig. S9g, S9h and S9i), thereby leading to the rapid capacity decay. In contrast, hierarchical porous $\delta\text{-MnO}_2$ nanoboxes catalyst can effectively improve the charge efficiency, thus ensuring the recovery of the electrode porosity (Fig. S9d, S9f) and the low resistance (Fig. S9g, S9h and S9i) during the charge process; as a consequence, enhanced cycle performance of the battery was obtained. The XRD and FTIR measurements of the electrode after the 5th charge process further confirm the fully decomposition of Li_2O_2 . However, two small peaks assigned to Li_2CO_3 and $\text{CH}_3\text{CO}_2\text{Li}$ were still observed, arising from the undecomposable nature of the side products.⁶⁹ (Fig. S8) The full capacity discharge–charge cycle performance of the Li-O_2 battery with flower-like MnO_2 electrode was also examined at 0.16 mA cm^{-2} for comparison. (Fig. S10a) There was no big difference between the MnO_2 nanoboxes and flower-like MnO_2 electrodes in the first discharge–charge cycle. However, more rapid discharge capacity decay was observed when using the flower-like MnO_2 electrode during the following cycles. This may be due to its relative small pore volume and narrow pore size distribution. (Fig. S10b) This result further highlights the superiority of hierarchical porous $\delta\text{-MnO}_2$ nanoboxes as the cathode of Li-O_2 battery.

The long cycle stability of the hierarchical porous $\delta\text{-MnO}_2$ nanoboxes electrode was evaluated following a widely used method by limiting the discharge capacity.^{15, 26} When the discharge potential dropped below 2.0 V, we considered the cell to be failed.

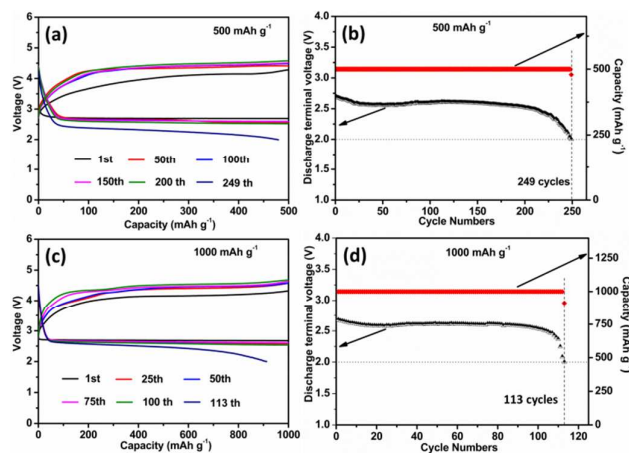


Fig. 5 Cyclic performance of hierarchical porous $\delta\text{-MnO}_2$ nanoboxes electrode at 0.16 mA cm^{-2} with limited capacity of 500 mAh g^{-1} (a, b) and 1000 mAh g^{-1} (c, d), respectively; (a, c) discharge–charge curves at different cycles; (b, d) capacity and terminal voltage of discharge vs. cycle numbers.

The selected cycled voltage profiles of the batteries with hierarchical porous $\delta\text{-MnO}_2$ nanoboxes electrode at the current density of 0.16 mA cm^{-2} with limited capacity of 500 mAh g^{-1} was shown in Fig. 5a. There was no loss of the discharge capacity of the battery cell with hierarchical porous $\delta\text{-MnO}_2$ nanoboxes electrode up to 249th cycles (Fig. 5b). In contrast, the cycle numbers were limited to 29 for the VX-72 carbon electrode (Fig. S11). When increasing the curtailing capacity to 1000 mAh g^{-1} , the cycle number of battery with hierarchical porous $\delta\text{-MnO}_2$ nanoboxes electrode can maintain for 112 cycles (Fig. 5c and 5d). To our knowledge this was one of the best cycle performances compared with state-of-the-art Li-O_2 batteries with manganese oxide based electrodes under similar testing condition.^{21, 26, 39, 70, 71} (Table S1) These results revealed that the hierarchical porous $\delta\text{-MnO}_2$ nanoboxes electrode had excellent long cycle stability.

4. Conclusion

In summary, we demonstrated a facile approach to synthesize hierarchical porous $\delta\text{-MnO}_2$ nanoboxes. The as-prepared products possessed hierarchical pore size and extremely large surface area up to $249.3 \text{ m}^2 \text{ g}^{-1}$. In comparison with the commercial Vulcan XC-72 carbon, the hierarchical porous $\delta\text{-MnO}_2$ nanoboxes as Li-O_2 battery cathode catalyst exhibited high catalytic activity towards both ORR and OER with reduced overpotentials up to 270 mV at 0.08 mA cm^{-2} . The battery also showed large specific capacity, enhanced rate performance and long cycle ability. At a rate of 0.16 mA cm^{-2} , the battery with hierarchical porous $\delta\text{-MnO}_2$ catalyst could demonstrate long cycle stability up to 248 cycles and 112 cycles with limited discharge capacity of 500 mAh g^{-1} and 1000 mAh g^{-1} , respectively. The improved battery performance was attributed to the intrinsic catalytic activity, hierarchical pore size distribution and large surface area of hierarchical porous $\delta\text{-MnO}_2$ nanoboxes. The superb performance of the hierarchical porous $\delta\text{-MnO}_2$ nanoboxes, together with the convenient fabrication method, suggests a new alternative to develop advanced cathode materials for Li-O_2 battery.

Acknowledgements

The authors acknowledge the financial support from the Singapore MOE grant R143-000-593-112.

Notes and references

^aSchool of Physics and Optoelectronic Engineering, Nanjing University of Information Science & Technology, Nanjing 210044, Jiangsu, China

^bDepartment of Chemistry, National University of Singapore 3 Science Drive 3, 117543, Singapore. E-mail: phycw@nus.edu.sg

^cDepartment of Physics National University of Singapore 2 Science Drive 3, 117542 Singapore

^dInstitute of Materials Research & Engineering, 3 Research Link, Singapore 117602, Singapore. E-mail: zl-liu@imre.a-star.edu.sg

^eNational University of Singapore (Suzhou) Research Institute, 377 Lin Quan Street, Suzhou Industrial Park, Jiangsu Prov. 215123, China

Author contributions

J. Zhang, Z. L. Liu and W. Chen designed the experiments. J. Zhang, Y. P. Luan and K. D. Yuan performed the experiments. Z. Y. Lyu, L. J. Wang, L. L. Xu and F. Pan discussed and commented on the experiments and results. J. Zhang, M. Lai, Z. L. Liu and W. Chen discussed and wrote the paper.

1. P. G. Bruce, S. A. Freunberger, L. J. Hardwick and J.-M. Tarascon, *Nat. Mater.*, 2012, **11**, 19-29.
2. J.-S. Lee, S. Tai Kim, R. Cao, N.-S. Choi, M. Liu, K. T. Lee and J. Cho, *Adv. Energy Mater.*, 2011, **1**, 34-50.
3. Y.-C. Lu, B. M. Gallant, D. G. Kwabi, J. R. Harding, R. R. Mitchell, M. S. Whittingham and Y. Shao-Horn, *Energy Environ. Sci.*, 2013, **6**, 750.
4. A. Kraysberg and Y. Ein-Eli, *J. Power Sources*, 2011, **196**, 886-893.
5. Y. C. Lu, E. J. Crumlin, G. M. Veith, J. R. Harding, E. Mutoro, L. Baggetto, N. J. Dudney, Z. Liu and Y. Shao-Horn, *Sci Rep*, 2012, **2**, 715.
6. J.-L. Shui, J. S. Okasinski, P. Kenesei, H. A. Dobbs, D. Zhao, J. D. Almer and D.-J. Liu, *Nat Commun*, 2013, **4**, 2255.
7. H.-K. Lim, H.-D. Lim, K.-Y. Park, D.-H. Seo, H. Gwon, J. Hong, W. A. Goddard, H. Kim and K. Kang, *J. Am. Chem. Soc.*, 2013, **135**, 9733-9742.
8. F. Cheng and J. Chen, *Chem. Soc. Rev.*, 2012, **41**, 2172-2192.
9. Y. Shao, S. Park, J. Xiao, J.-G. Zhang, Y. Wang and J. Liu, *ACS Catal.*, 2012, **2**, 844-857.
10. A. C. Luntz and B. D. McCloskey, *Chem. Rev.*, 2014, **114**, 11721-11750.
11. B. D. McCloskey, R. Scheffler, A. Speidel, D. S. Bethune, R. M. Shelby and A. C. Luntz, *J. Am. Chem. Soc.*, 2011, **133**, 18038-18041.
12. W. Zhang, J. Zhu, H. Ang, Y. Zeng, N. Xiao, Y. Gao, W. Liu, H. Hng and Q. Yan, *Nanoscale*, 2013, **5**, 9651-9658.
13. Y.-C. Lu, H. A. Gasteiger and Y. Shao-Horn, *J. Am. Chem. Soc.*, 2011, **133**, 19048-19051.
14. H.-D. Lim, H. Song, J. Kim, H. Gwon, Y. Bae, K.-Y. Park, J. Hong, H. Kim, T. Kim, Y. H. Kim, X. Lepró, R. Ovalle-Robles, R. H. Baughman and K. Kang, *Angew. Chem. Int. Ed.*, 2014, **53**, 3926-3931.
15. J.-J. Xu, Z.-L. Wang, D. Xu, F.-Z. Meng and X.-B. Zhang, *Energy Environ. Sci.*, 2014, **7**, 2213-2219.
16. H. Nie, H. Zhang, Y. Zhang, T. Liu, J. Li and Q. Lai, *Nanoscale*, 2013, **5**, 8484-8487.
17. X. Lin, Y. Shang, T. Huang and A. Yu, *Nanoscale*, 2014, **6**, 9043-9049.
18. Y. Cui, Z. Wen and Y. Liu, *Energy Environ. Sci.*, 2011, **4**, 4727-4734.
19. H. Wang, Y. Yang, Y. Liang, G. Zheng, Y. Li, Y. Cui and H. Dai, *Energy Environ. Sci.*, 2012, **5**, 7931-7935.
20. J. Zhang, Y. Zhao, X. Zhao, Z. Liu and W. Chen, *Sci. Rep.*, 2014, **4**.
21. A. Débart, A. J. Paterson, J. Bao and P. G. Bruce, *Angew. Chem. Int. Ed.*, 2008, **47**, 4521-4524.
22. S. Ida, A. K. Thapa, Y. Hidaka, Y. Okamoto, M. Matsuka, H. Hagiwara and T. Ishihara, *J. Power Sources*, 2012, **203**, 159-164.
23. L. Trahey, N. K. Karan, M. K. Y. Chan, J. Lu, Y. Ren, J. Greeley, M. Balasubramanian, A. K. Burrell, L. A. Curtiss and M. M. Thackeray, *Adv. Energy Mater.*, 2013, **3**, 75-84.
24. L. L. Zhang, Z. L. Wang, D. Xu, J. J. Xu, X. B. Zhang and L. M. Wang, *Chin. Sci. Bull.*, 2012, **57**, 4210-4214.
25. T. T. Truong, Y. Liu, Y. Ren, L. Trahey and Y. Sun, *ACS Nano*, 2012, **6**, 8067-8077.
26. Y. Qin, J. Lu, P. Du, Z. Chen, Y. Ren, T. Wu, J. T. Miller, J. Wen, D. J. Miller, Z. Zhang and K. Amine, *Energy Environ. Sci.*, 2013, **6**, 519.
27. L. L. Zhang, F. F. Zhang, G. Huang, J. W. Wang, X. C. Du, L. Qin and L. M. Wang, *J. Power Sources*, 2014, **261**, 311-316.
28. S. Y. Liu, Y. G. Zhu, J. Xie, Y. Huo, H. Y. Yang, T. J. Zhu, G. S. Cao, X. B. Zhao and S. C. Zhang, *Adv. Energy Mater.*, 2014, **4**, 9.
29. Y. Cao, Z. K. Wei, J. He, J. Zang, Q. Zhang, M. S. Zheng and Q. F. Dong, *Energy Environ. Sci.*, 2012, **5**, 9765-9768.
30. Y. Yu, B. Zhang, Y. B. He, Z. D. Huang, S. W. Oh and J. K. Kim, *J. Mater. Chem. A*, 2013, **1**, 1163-1170.
31. Y. Yang, M. Shi, Y. S. Li and Z. W. Fu, *J. Electrochem. Soc.*, 2012, **159**, A1917-A1921.
32. X. Hu, X. Han, Y. Hu, F. Cheng and J. Chen, *Nanoscale*, 2014, **6**, 3522-3525.
33. X. F. Hu, X. P. Han, Y. X. Hu, F. Y. Cheng and J. Chen, *Nanoscale*, 2014, **6**, 3522-3525.
34. A. K. Thapa, T. H. Shin, S. Ida, G. U. Sumanasekera, M. K. Sunkara and T. Ishihara, *J. Power Sources*, 2012, **220**, 211-216.
35. K. N. Jung, A. Riaz, S. B. Lee, T. H. Lim, S. J. Park, R. H. Song, S. Yoon, K. H. Shin and J. W. Lee, *J. Power Sources*, 2013, **244**, 328-335.
36. S.-Y. Liu, G. Wang, J. Xie, F. Tu, H. Yang, S. Zhang, T. Zhu, G. S. Cao and X. B. Zhao, *Nanoscale*, 2015, DOI: 10.1039/C5NR01344E.
37. L. Jin, L. P. Xu, C. Morein, C. H. Chen, M. Lai, S. Dharmarathna, A. Doble and S. L. Suib, *Adv. Funct. Mater.*, 2010, **20**, 3373-3382.
38. P. Zhang, D. Sun, M. He, J. Lang, S. Xu and X. Yan, *ChemSusChem*, 2015, **8**, 1972-1979.
39. S. Liu, Y. Zhu, J. Xie, Y. Huo, H. Y. Yang, T. Zhu, G. Cao, X. Zhao and S. Zhang, *Adv. Energy Mater.*, 2014, **4**, 9.

40. S. Liu, G. Wang, F. Tu, J. Xie, H. Y. Yang, S. Zhang, T. Zhu, G. Cao and X. Zhao, *Nanoscale*, 2015, **7**, 9589-9596.
41. J.-J. Xu, Z.-L. Wang, D. Xu, L.-L. Zhang and X.-B. Zhang, *Nat Commun*, 2013, **4**, 2438.
42. H. D. Lim, K. Y. Park, H. Song, E. Y. Jang, H. Gwon, J. Kim, Y. H. Kim, M. D. Lima, R. Ovalle Robles, X. Lepro, R. H. Baughman and K. Kang, *Adv Mater*, 2013, **25**, 1348-1352.
43. H.-D. Lim, H. Song, H. Gwon, K.-Y. Park, J. Kim, Y. Bae, H. Kim, S.-K. Jung, T. Kim, Y. H. Kim, X. Lepro, R. Ovalle-Robles, R. H. Baughman and K. Kang, *Energy Environ. Sci.*, 2013, **6**, 3570.
44. J.-J. Xu, D. Xu, Z.-L. Wang, H.-G. Wang, L.-L. Zhang and X.-B. Zhang, *Angew. Chem. Int. Ed.*, 2013, **52**, 3887-3890.
45. N. Ding, S. W. Chien, T. S. A. Hor, R. Lum, Y. Zong and Z. Liu, *J. Mater. Chem. A*, 2014, **2**, 12433-12441.
46. Z. Zhang, J. Bao, C. He, Y. Chen, J. Wei and Z. Zhou, *Adv. Funct. Mater.*, 2014, **24**, 6826-6833.
47. L. Zhang, L. Shi, L. Huang, J. Zhang, R. Gao and D. Zhang, *ACS Catal.*, 2014, **4**, 1753-1763.
48. L. Hu and Q. Chen, *Nanoscale*, 2014, **6**, 1236-1257.
49. L. Hu, P. Zhang, H. Zhong, X. Zheng, N. Yan and Q. Chen, *Chem. Eur. J*, 2012, **18**, 15049-15056.
50. X.-Y. Yu, L. Yu, H. B. Wu and X. W. Lou, *Angew. Chem. Int. Ed.*, 2015, **54**, 5331-5335.
51. L. Zhang, H. B. Wu and X. W. Lou, *J. Am. Chem. Soc.*, 2013, **135**, 10664-10672.
52. L. Zhang, H. B. Wu, S. Madhavi, H. H. Hng and X. W. Lou, *J. Am. Chem. Soc.*, 2012, **134**, 17388-17391.
53. L. Zhang, H. B. Wu, R. Xu and X. W. Lou, *CrystEngComm*, 2013, **15**, 9332-9335.
54. L. Hu, N. Yan, Q. Chen, P. Zhang, H. Zhong, X. Zheng, Y. Li and X. Hu, *Chem. Eur. J*, 2012, **18**, 8971-8977.
55. L. Hu, Y. Huang and Q. Chen, *J. Alloys Compd.*, 2013, **559**, 57-63.
56. L. Hu, Y. Huang, F. Zhang and Q. Chen, *Nanoscale*, 2013, **5**, 4186-4190.
57. L. Hu, J.-y. Mei, Q.-w. Chen, P. Zhang and N. Yan, *Nanoscale*, 2011, **3**, 4270-4274.
58. L. Hu, P. Zhang, Q.-w. Chen, N. Yan and J.-y. Mei, *Dalton Trans.*, 2011, **40**, 5557-5562.
59. D. P. Dubal, D. S. Dhawale, R. R. Salunkhe and C. D. Lokhande, *J. Mater. Chem.*, 2010, **647**, 60-65.
60. J. Moon, M. Awano, H. Takagi and Y. Fujishiro, *J. Mater. Res.*, 1999, **14**, 4594-4601.
61. A. Ramirez, P. Hillebrand, D. Stellmach, M. M. May, P. Bogdanoff and S. Fiechter, *J. Phys. Chem. C*, 2014, **118**, 14073-14081.
62. H. Chen, X. Dong, J. Shi, J. Zhao, Z. Hua, J. Gao, M. Ruan and D. Yan, *J. Mater. Chem.*, 2007, **17**, 855-860.
63. F. Grote, R.-S. Kühnel, A. Balducci and Y. Lei, *Appl. Phys. Lett.*, 2014, **104**, 053904.
64. V. Subramanian, H. Zhu, R. Vajtai, P. M. Ajayan and B. Wei, *The Journal of Physical Chemistry B*, 2005, **109**, 20207-20214.
65. W. Xiao, D. Wang and X. W. Lou, *J. Phys. Chem. C*, 2009, **114**, 1694-1700.
66. M.-W. Xu, D.-D. Zhao, S.-J. Bao and H.-L. Li, *J. Solid State Electrochem.*, 2007, **11**, 1101-1107.
67. J. Zhang, L. Wang, L. Xu, X. Ge, X. Zhao, M. Lai, Z. Liu and W. Chen, *Nanoscale*, 2015, **7**, 720-726.
68. M. M. Ottakam Thotiyl, S. A. Freunberger, Z. Peng, Y. Chen, Z. Liu and P. G. Bruce, *Nat. Mater.*, 2013, **12**, 1050-1056.
69. K.-N. Jung, J.-I. Lee, W. B. Im, S. Yoon, K.-H. Shin and J.-W. Lee, *Chem. Commun.*, 2012, **48**, 9406-9408.
70. Y. Cao, Z. Wei, J. He, J. Zang, Q. Zhang, M. Zheng and Q. Dong, *Energy Environ. Sci.*, 2012, **5**, 9765-9768.
71. X. Han, F. Cheng, C. Chen, Y. Hu and J. Chen, *Nano Res.*, 2014, **8**, 156.

Supporting Information

Synthesis of hierarchical porous δ -MnO₂ nanoboxes as an efficient catalyst for rechargeable Li–O₂ battery

Jian Zhang,^{a,b} Yanping Luan,^b Zhiyang Lyu,^b Liangjun Wang,^c Leilei Xu,^b Kaidi Yuan,^c Feng Pan,^b Min Lai,^a Zhaolin Liu,^{*d} and Wei Chen ^{*bce}

a. School of Physics and Optoelectronic Engineering, Nanjing University of Information Science & Technology, Nanjing 210044, Jiangsu, China

b. Department of Chemistry, National University of Singapore 3 Science Drive 3, 117543, Singapore. E-mail: phycw@nus.edu.sg

c. Department of Physics National University of Singapore 2 Science Drive 3, 117542 Singapore

d. Institute of Materials Research & Engineering, 3 Research Link, Singapore 117602, Singapore. E-mail: zl-liu@imre.a-star.edu.sg

e. National University of Singapore (Suzhou) Research Institute, 377 Lin Quan Street, Suzhou Industrial Park, Jiangsu Prov. 215123, China

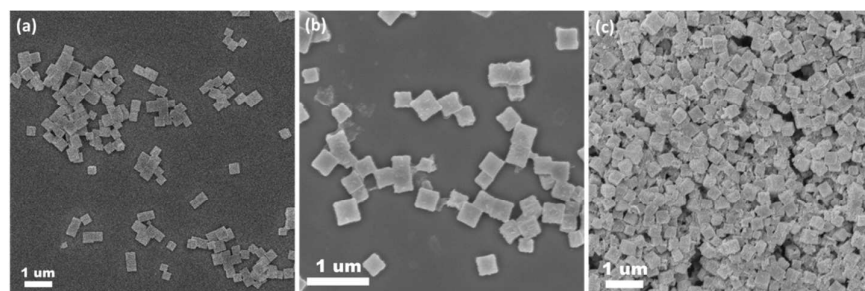


Fig. S1. SEM images of the obtained (a) nanocube-like PBAs precursors, (b) porous Mn_3O_4 nanoboxes and (c) hierarchical porous $\delta\text{-MnO}_2$ nanoboxes.

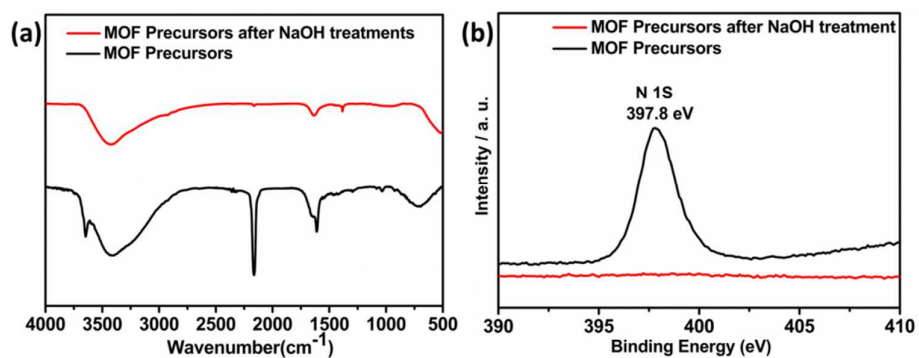


Fig. S2. (a) FT-IR and (b) N 1s XPS spectra of the PBAs precursor before (black) and after (red) NaOH treatment.

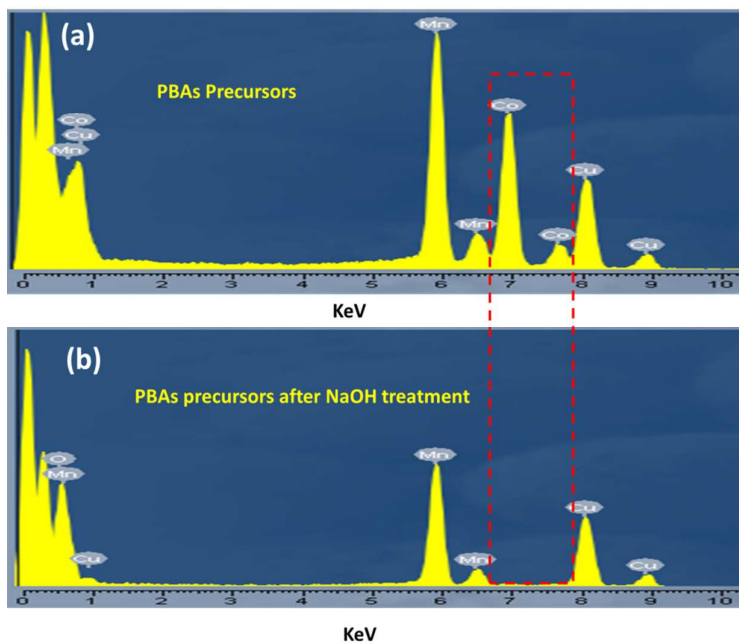


Fig. S3. EDX spectra of the PBAs precursors (a) before and (b) after the NaOH treatment.

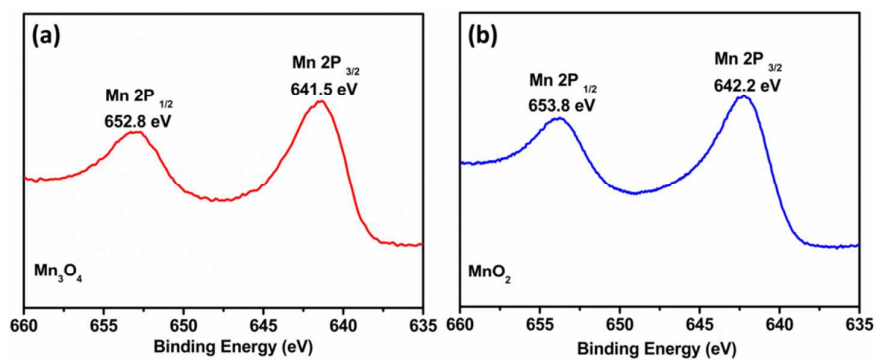


Fig. S4. XPS survey of (a) porous Mn₃O₄ nanoboxes and (b) hierarchical porous δ -MnO₂ nanoboxes.

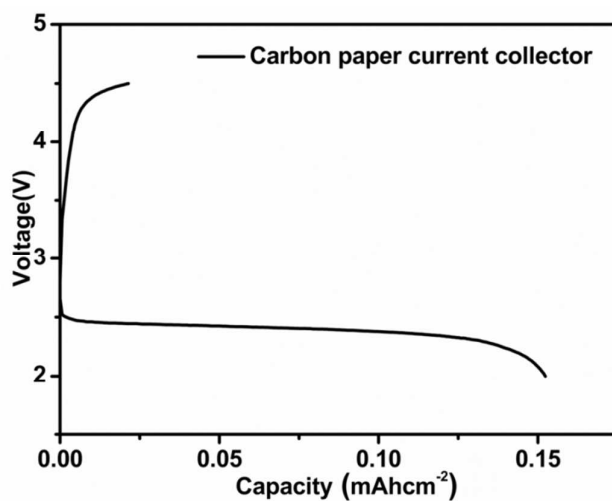


Fig. S5. Discharge-charge curves of Li-O₂ batteries with blank carbon paper current collector.

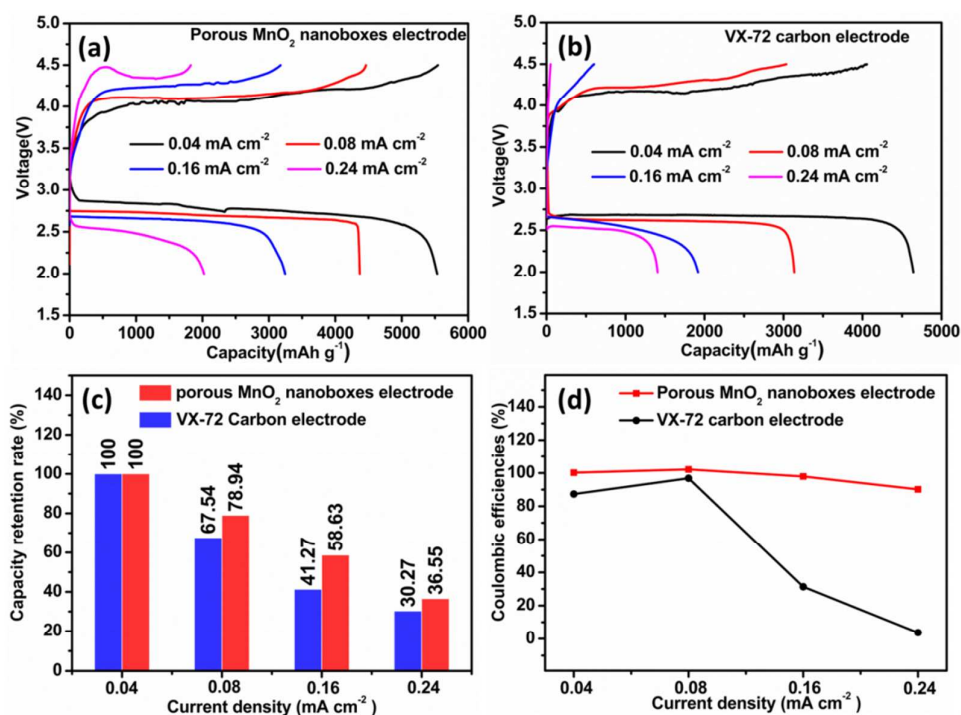


Fig. S6. First discharge-charge curves of Li-O₂ batteries with (a) hierarchical porous δ -MnO₂ nanoboxes and (b) VX-72 carbon electrodes at various current densities; (c) Discharge capacity retention of Li-O₂ battery cells with different electrodes at various current densities; (d) Coulombic efficiency of Li-O₂ batteries with different electrodes at various current density.

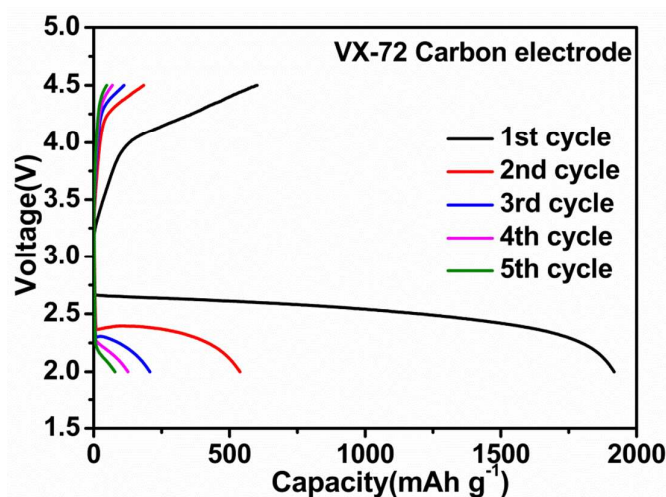


Fig. S7. Discharge-charge curves of Li-O₂ batteries with VX-72 carbon electrode at 0.16 mA cm⁻².

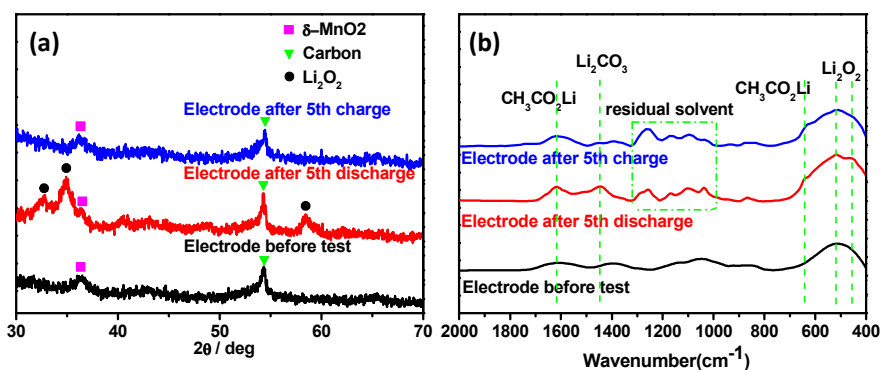


Fig. S8. (a) XRD pattern and (b) FTIR spectrum of the electrode at different states.

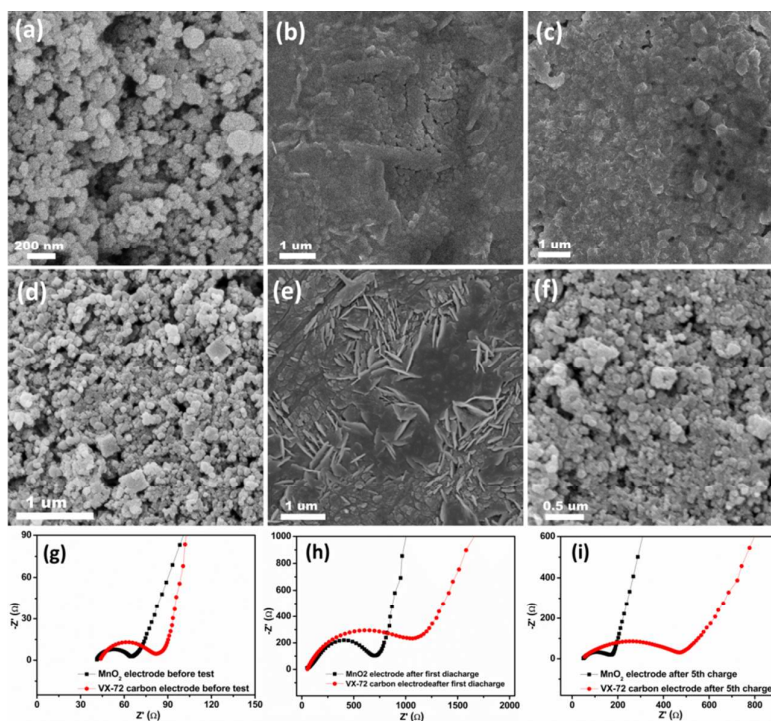


Fig. S9. SEM images of the VX-72 carbon electrode (a, b, c) and hierarchical porous δ -MnO₂ nanoboxes electrode (d, e, f), before test (a, d), after 5th discharge (b, e) and after 5th charge (c, f); (g), (h), (i) electrochemical impedance spectra of Li–O₂ batteries with the hierarchical porous δ -MnO₂ nanoboxes and VX-72 carbon electrodes at different discharge–charge states.

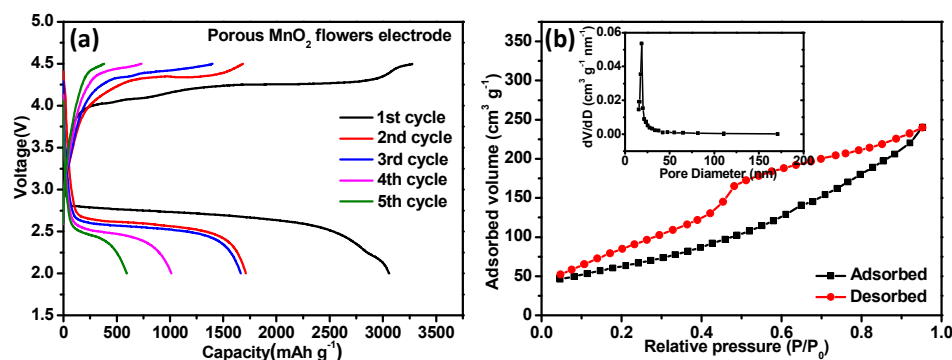


Fig. S10. (a) Discharge-charge curves of Li-O₂ batteries with hierarchical porous δ -MnO₂ nanoboxes electrode at 0.16 mA cm⁻²; (b) Nitrogen adsorption-desorption isotherms and pore size distribution (inset) of the flower-like δ -MnO₂. The BET surface area is about 229.6 m² g⁻¹ and the pore volume is 0.340 cm³ g⁻¹

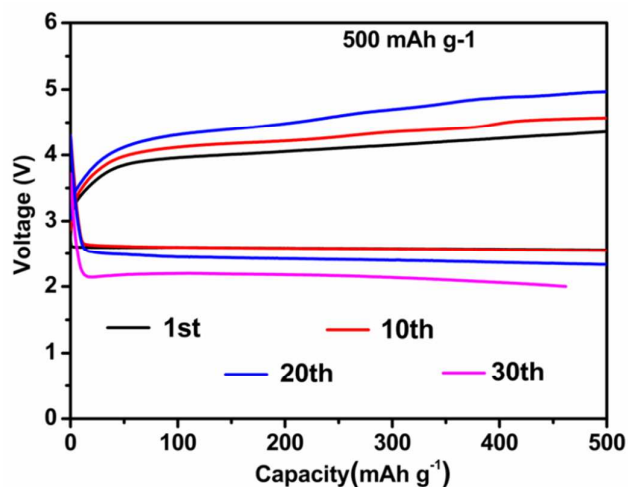


Fig. S11. Cyclic performance of the VX-72 carbon electrode at 0.16 mA cm⁻² with limited capacity of 500 mAh g⁻¹.

Table S1. Summary of surface area of manganese-based catalysts and their related Li-O₂ batteries performance.

Catalyst	BET surface area (m ² g ⁻¹)	Overpotential (V)	Maximum capacity based on total mass (mAh g ⁻¹)	Rate capacity (mAh g ⁻¹)	Cycle performance	Ref.
α-MnO ₂	--	1.4 at 70 mA g ⁻¹	730 at 70 mA g ⁻¹	--	--	[1]
δ-MnO ₂ /3-D graphene	108	1.4 V at 0.083 mA cm ⁻²	3660 at 48 mA g ⁻¹	700 at 387 mA g ⁻¹	132 cycles at 1000 mA g ⁻¹	[2]
α-MnO ₂ /graphene	71	0.99 at 0.06 mA cm ⁻²	2304 at 100mA g ⁻¹	--	25cycles at 3000 mA g ⁻¹	[3]
α-MnO ₂ /porous carbon	70	1.38 at 100 mA g ⁻¹	1400 at 100mA g ⁻¹	--	60 cycles at 500 mA g ⁻¹	[4]
ε-MnO ₂ /Ni foam	125.57	1.25 at 10 mA g ⁻¹	7000 at 100mA g ⁻¹	6300 at 500 mA g ⁻¹	120 cycles at 1000 mA g ⁻¹	[5]
Our sample	249.3	1.36 at 0.08 mA cm ⁻²	5533 at 50 mA g ⁻¹	2022 at 200 mA g ⁻¹	248 cycles at 500 mAh g ⁻¹ 113 cycles at 1000 mAh g ⁻¹	

[1] A. Débart, A. J. Paterson, J. Bao, P. G. Bruce, *Angew. Chem. Int. Ed.* **2008**, 47, 4521.

[2] S. Liu, Y. Zhu, J. Xie, Y. Huo, H. Y. Yang, T. Zhu, G. Cao, X. Zhao, S. Zhang, *Adv. Energy Mater.* **2014**, 4, 9.

[3] Y. Cao, Z. Wei, J. He, J. Zang, Q. Zhang, M. Zheng, Q. Dong, *Energy Environ. Sci.* **2012**, 5, 9765.

[4] Y. Qin, J. Lu, P. Du, Z. Chen, Y. Ren, T. Wu, J. T. Miller, J. Wen, D. J. Miller, Z. Zhang, K. Amine, *Energy Environ. Sci.* **2013**, 6, 519.

[5] X. Hu, X. Han, Y. Hu, F. Cheng, J. Chen, *Nanoscale* **2014**, 6, 3522.